Supplement of

Unexpected high volatile organic compounds emission from vehicles on the Tibetan Plateau

Weichao Huang[1#], Sihang Wang[2#], Peng Cheng[1*], Bingna Chen[1], Bin Yuan[2*], Pengfei Yu[2], Haichao Wang[3], Nan Ma[2], Mei Li[1], Keding Lu[4,5]

[1]*College of Environment and Climate, Institute of Mass Spectrometry and Atmospheric Environment, Guangdong Provincial Engineering Research Center for Online Source Apportionment System of Air Pollution, Guangdong-Hongkong-Macau Joint Laboratory of Collaborative Innovation for Environmental Quality, Jinan University, Guangzhou 510632, China*

[2]*College of Environment and Climate, Institute for Environmental and Climate Research, Guangdong-Hongkong-Macau Joint Laboratory of Collaborative Innovation for Environmental Quality, Jinan University, Guangzhou 511443, China*

[3]*School of Atmospheric Sciences, Sun Yat-sen University, Zhuhai 519082, China*

[4]*State Key Joint Laboratory of Environmental Simulation and Pollution Control, College of Environmental Sciences and Engineering, Peking University, Beijing, 100871, China*

[5]*International Joint Laboratory of Regional Pollution Control (IJRC), Peking University, Beijing, 100871, China*

[*]Correspondence to: Peng Cheng (chengp@jnu.edu.cn); Bin Yuan (byuan@jnu.edu.cn)

[#]These authors contributed equally to this work.

Number of pages: 35
Number of Figures: 13
Number of Tables: 7

Text S1. Instrumentation

Offline analysis of VOCs was conducted using an analytical system (Model TH-300B, Tianhong, Inc., Wuhan, China). This system comprises a pretreatment unit (Model TH-PKU 300B), followed by a gas chromatograph (GC) (Model 7820A, Agilent Technologies) equipped with a flame ionization detector (FID), and an Agilent 5977E quadrupole mass spectrometer detector (MSD) for compound detection and analysis.

The analytical procedure commenced with the filtration of samples, followed by the removal of water and CO_2, prior to their introduction into the cryotrap at a flow rate of 60 ml/min. Within the cryotrap, the samples were rapidly cooled to a temperature of -150 ℃ and subsequently heated to 110 ℃. This thermal manipulation facilitated the identification of VOCs using FID and MSD in the selected ion monitoring mode. For the quantification of C_2-C_5 hydrocarbons, the FID utilized a porous layer open tubular phase column. Conversely, the MSD, equipped with a semi-polar DB-624 column, was tasked with detecting C_5-C_{12} hydrocarbons. The DB-624 capillary column's analytical cycle spanned 33 min, beginning with an initial temperature hold at 30 ℃ for 3 min. This was followed by a temperature ramp to 180 ℃ at a rate of 6.0 ℃/min, which was then maintained for 5 min. The system maintained a carrier gas flow rate of 1.3 mL/min, while the inlet temperature was held constant at 200 ℃. At the junction where the GC system interfaces with the MS, the temperature was set at 280 ℃. The ion source for the mass spectrometry employed electron ionization (EI) technique.

The analytical system was calibrated with internal and external standards. The target compounds were identified by retention time and mass spectrometry, and quantified by external calibration. MSD signal is the main signal for C_6-C_{12} hydrocarbons, and FID signal is the main signal for C_2-C_5 hydrocarbons. The internal standard compound standard gas provided by Linde Gas company, USA had a concentration volume fraction of 1.0 ppmv and was diluted to 4.0 ppbv. The calibration standards were prepared by diluting 1.0 ppmv Photochemical Assessment Monitoring Stations (PAMS) standard mixture and TO-15 standard mixture from Linde Gas, USA

to 0.40, 0.80, 1.2, 2.0, 3.2, 4.0 ppbv (Du et al., 2018). The correlation coefficients for the 90 species detected in this study are presented in Table S1.

Text S2. Positive Matrix Factorization and Non-Negative Least Squares Analysis

In this study, we utilized the positive matrix factorization (PMF) 5.0 developed by the US EPA to analyze the sources of VOCs (Paatero and Tapper, 1994). The fundamental principle of the PMF 5.0 model is to decompose the sample component concentration matrix into a source contribution matrix, a source component profile matrix, and a residual matrix. It employs an iterative algorithm to minimize the objective function Q, thereby determining the optimal analytical result. The computational formula is as shown in Eq. (S3) and Eq. (S4):

$$x_{ij} = \sum_{k=1}^{p} g_{ik} f_{kj} + e_{ij} \tag{S3}$$

$$Q = \sum_{i=1}^{n} \sum_{j=1}^{m} \left[\frac{x_{ij} - \sum_{k=1}^{p} g_{ik} f_{ki}}{u_{ij}} \right]^2 \tag{S4}$$

In this equation, x_{ij} represents the concentration of component j in sample i; p is the number of pollution sources; g_{ik} is the contribution of pollution source k to sample i; f_{ki} is the content of component j in pollution source k; e_{ij} is the residual; Q is the cumulative residual; and u_{ij} is the uncertainty of x_{ij}.

The PMF 5.0 model requires data on receptor point detection concentration and uncertainty. The uncertainty calculation formula is as shown in Eq. (S5).

$$Unc = \sqrt{(EF \times c)^2 + (0.5 \times MDL)^2} \tag{S5}$$

In this equation, EF represents the error fractionis, is typically set between 5% to 20%. In this study, the EF value is set at 10%; c is the detection concentration, in $ug \cdot m^{-3}$; and MDL is the method detection limit, in $ug \cdot m^{-3}$.

Table S3 displays the configuration parameters used for the PMF run. Prior to executing the PMF, weights must be assigned to the species involved in the model computations. This study uses the signal-to-noise ratio (S/N) to categorize these species, with categories designated as "Bad" for S/N less than 0.5, "Weak" for S/N between 0.5 and 1.0, and "Strong" for S/N greater than 1.0. Species with relatively low sample concentrations are also designated as "Bad," and those classified as "Bad" are typically excluded from computations. Ultimately, 66 species were included in the PMF model calculations. Considering that the aim of this study is to discern the source contributions of evaporative and exhaust emissions in the tunnel environment via the PMF model, our primary focus is centered on these two emission sources. To accurately reflect the realities of the tunnel environment, we introduced necessary constraints when running the model. These primarily involved certain species associated with non-vehicular sources (Factor 3), ensuring that our model's outcomes align with the actual tunnel conditions.

To further substantiate the results derived from the PMF analysis, we also employed the Non-negative Least Squares (NNLS) regression approach in this study. In the NNLS model, one independent variable signifies the evaporative species n-butane (X_1), and another independent variable symbolizes the combustion species ethylene (X_2). The dependent variable Y comprises the remaining species. The computational formula is as shown in Eq. (S6):

$$Min \sum_i (Y_i - aX_1 - bX_2 - c)^2$$

$$subject\ to\ a > 0,\ b > 0,\ and\ c \geq 0 \qquad \text{(S6)}$$

In this formulation, a and b are the relative contribution coefficients of n-butane and ethylene to Y, respectively, while c represents the relative contribution of other sources to Y. Ensuring that the coefficients remain non-negative aligns with the physical reality that species cannot exert a negative influence on the dependent variable. The objective of the analysis is to find the optimal contribution coefficients that best fit the

observed data, thereby unveiling the relative contribution of each species.

Text S3. Clapeyron equation for calculating boiling point

To calculate the boiling points of n-pentane at high altitudes with lower atmospheric pressures, we employ the Clausius-Clapeyron equation. This equation relates the change in vapor pressure with temperature, allowing us to determine the boiling point at various pressures. The equation is given by:

$$ln\left(\frac{P_2}{P_1}\right) = \frac{-\Delta H}{R}\left(\frac{1}{T_2} - \frac{1}{T_1}\right) \quad \text{(S7)}$$

where, P_1 is the standard atmospheric pressure (101325 Pa). T_1 is the boiling point of the VOC under standard conditions, expressed in K. P_2 is the atmospheric pressure at 4750 m, expressed in 55857 Pa. T_2 is the boiling point of n-pentane at the pressure. ΔH is the heat of vaporization of n-pentane, J/mol. R is the universal gas constant (8.314 J/(mol·K)). For n-pentane, the normal boiling point (T_1=308.4 K) and the heat of vaporization (ΔH=26900 J/mol) are obtained from the ChemSpider website (2024). As a result, the temperature of n-pentane at an altitude of 4750 m was calculated to be 291.8 K, equivalent to 19°C.

Text S4. Special tunnel sample

In the course of this study, certain unique conditions were encountered that necessitated the exclusion of specific samples from the analysis. Among the 46 samples collected across 10 different high-altitude tunnels, a subset of these samples were influenced by atypical vehicular emission events. Specifically, 5 samples were affected by the passage of heavy-duty diesel vehicles or a surge of traffic near our mobile measurement vehicle at the time of summa canister activation, resulting in anomalously high VOC measurements. Thus, these samples essentially captured a fresh, instantaneous emission of VOCs, rather than VOC concentrations that had been evenly mixed in the tunnel air over time. Additionally, the collection timing of 4 samples may

not have been ideal, as they were gathered during periods of uncharacteristically low CO and CO_2 concentrations in some tunnels. During the specified sampling periods, a discrepancy was observed between the VOC concentrations measured and the corresponding levels of CO and CO_2 recorded by the online instruments. This misalignment led to anomalously high values in the calculated emission factors (EF) and emission ratios (ER). This inconsistency highlights the inherent uncertainties encountered when integrating offline and online data in environmental analysis, particularly in the context of dynamic vehicular emissions. These 9 samples, identified as outliers due to their non-representative nature, were excluded from the EF and ER analysis to maintain data integrity and ensure the reliability of our EF and ER, thereby presenting a more accurate representation of typical vehicular emissions at varying altitudes. The criteria for exclusion were grounded in a comprehensive evaluation of the CO and CO_2 time series data, as well as the specific real-time conditions recorded by the driving recorder during each sampling event (Fig S13a).

Table S1. Detailed information of the test tunnels at high-altitude areas.

Altitude group/m	Atmospheric Pressure/kPa	Altitude/m	Tunnel	Length/m	Type	Direction	Valid samples
4750	55.9	4750	Mila Mountain Tunnel	5727	Highway two-bore one-way	West - East	3
						East - West	3
4200	60.1	4200	Yangbajing No. 2 Tunnel	6275	Highway two-bore one-way	West - East	3
						East - West	4
		4180	Songduo Tunnel	2195	Highway two-bore one-way	East - West	1
3600	64.9	3550	Gala Mountain Tunnel	2700	Highway two-bore one-way	North - South	3
						South - North	2
		3650	Bangga Tunnel	2000	Highway two-bore one-way	West - East	4
						East - West	3
3400	66.6	3400	Gongbujiangda Tunnel	1275	Highway two-bore one-way	West - East	2
						East - West	4
		3300	Laohuzui Tunnel	461	Rural road single-bore two-way	North - South	1
						South - North	1
3000	70.1	2980	Bayi Tunnel	650 575	Highway two-bore one-way	West - East	2
						East - West	3
2000	79.5	2040	Parlung No. 1 Tunnel	1390	National road single-bore two-way	West - East	1
						East - West	2
		2020	Parlung No. 2 Tunnel	2087	National road single-bore two-way	West - East	2
						East - West	2

158 **Table S2.** The correlation of VOC species detected by the GC-FID/MS.

VOC species	MDL (ppb)	RE (%)	R^2
Ethane	0.050	0.07	1.0000
Propane	0.021	0.02	1.0000
n-Butane	0.030	1.08	0.9999
i-Butane	0.012	1.17	0.9997
n-Pentane	0.026	-16.60	0.9967
i-Pentane	0.012	-10.83	0.9984
Cyclopentane	0.026	-16.36	0.9984
2,2-Dimethylbutane	0.007	-12.36	0.9982
2,3-Dimethylbutane	0.005	-7.11	0.9967
2-Methylpentane	0.005	-12.37	0.9988
3-Methylpentane	0.007	-14.10	0.9983
Cyclohexane	0.004	-12.89	0.9985
Methylcyclopentane	0.008	-13.52	0.9981
n-Hexane	0.016	-12.64	0.9984
2,3-Dimethylpentane	0.016	-13.63	0.9983
2,4-Dimethylpentane	0.005	-13.61	0.9981
2-Methylhexane	0.008	-13.69	0.9979
3-Methylhexane	0.006	-13.28	0.9982
Methylcyclohexane	0.008	-14.16	0.9983
n-Heptane	0.007	-13.70	0.9980
2,2,4-Trimethylpentane	0.003	-13.24	0.9984
2,3,4-Trimethylpentane	0.008	-14.14	0.9983
2-Methylheptane	0.008	-14.75	0.9987
3-Methylheptane	0.009	-14.47	0.9983
n-Octane	0.121	-15.55	0.9985
n-Nonane	0.021	-19.35	0.9983
n-Decane	0.030	-35.78	0.9962

n-Undecane	0.020	-50.45	0.9804
n-Dodecane	0.020	-50.63	0.9797
Ethylene	0.030	0.06	1.0000
Propene	0.025	0.60	1.0000
1,3-Butadiene	0.030	-10.79	0.9961
1-Butene	0.030	-13.35	0.9979
cis-2-Butene	0.023	-9.67	0.9984
trans-2-Butene	0.031	-20.39	0.9991
1-Pentene	0.009	-13.42	0.9980
Isoprene	0.015	-13.72	0.9987
cis-2-Pentene	0.008	-12.90	0.9987
trans-2-Pentene	0.008	-13.35	0.9979
1-Hexene	0.011	-14.05	0.9984
Acetylene	0.048	4.82	1.0000
Benzene	0.007	-13.38	0.9980
Toluene	0.005	-14.76	0.9984
Ethylbenzene	0.003	-17.48	0.9985
Styrene	0.013	-21.72	0.9982
o-Xylene	0.003	-19.83	0.9985
m/p-Xylene	0.004	15.37	0.9986
1,2,3-Trimethylbenzene	0.002	-42.71	0.9955
1,2,4-Trimethylbenzene	0.003	-40.18	0.9970
1,3,5-Trimethylbenzene	0.004	-36.96	0.9981
n-Propylbenzene	0.016	-32.10	0.9983
i-Propylbenzene	0.020	-26.42	0.9984
o-Ethyltoluene	0.020	-36.06	0.9980
m-Ethyltoluene	0.020	-34.17	0.9984
p-Ethyltoluene	0.020	-36.96	0.9981
Bromomethane	0.004	-8.86	0.9963

Chloroform	0.002	-13.43	0.9986
Chloromethane	0.020	-7.61	0.9955
Dibromochloromethane	0.030	-16.05	0.9988
Dichloromethane	0.038	-10.50	0.9998
Tribromomethane	0.004	-19.34	0.9983
Freon-11	0.016	-4.88	0.9970
1,1,2,2-tetrachloroethane	0.008	-34.65	0.9964
Freon-114	0.130	-13.01	0.9927
1,1,2-Trichloroethane	0.011	-16.72	0.9978
1,1-Dichloroethane	0.010	-13.25	0.9982
1,1-Dichloroethylene	0.010	-11.73	0.9988
Freon-113	0.011	-91.22	0.9990
1,2-Dibromoethane	0.010	-17.20	0.9977
1,2-Dichloroethane	0.019	-13.84	0.9993
Chloroethane	0.023	-12.08	0.9966
Tetrachloroethylene	0.008	-16.21	0.9980
Trichloroethylene	0.002	-13.79	0.9977
Vinyl chloride	0.010	-12.52	0.9945
cis-1,2-Dichloroethylene	0.015	-16.50	0.9968
trans-1,2-Dichloroethylene	0.015	-12.39	0.9988
1,2-Dichloropropane	0.013	-14.61	0.9978
trans-1,3-Dichloropropene	0.012	-18.14	0.9985
Chlorobenzene	0.008	-15.85	0.9982
o-Dichlorobenzene	0.006	-34.47	0.9971
m-Dichlorobenzene	0.006	-28.59	0.9980
p-Dichlorobenzene	0.004	-27.33	0.9978
Ethanol	0.131	-23.68	0.9937
Acetone	0.011	-36.23	0.9890
Acrolein	0.022	-12.84	0.9987

2-Butanone	0.014	-13.89	0.9982
Tetrahydrofuran	0.005	-12.84	0.9987
Vinyl acetate	0.021	-13.63	0.9981
Methyl isobutyl ketone	0.004	-14.31	0.9984
Methyl tertiary-butyl ether	0.025	-49.89	0.9895

159
160

161 **Table S3.** Configurations of the PMF model runs.

Parameter/ PMF run	Source of tunnel VOCs
N species	66
N samples	46
N factors	3
Number of runs	5
Uncertainty	10%
Treatment of data below minimum detection limit (MDL)	No treatment
Seed Value	Random
Category	Bad: Styrene, Bromomethane, Dibromochloromethane, Tribromomethane, Freon-11, 1,1,2,2-tetrachloroethane, Freon-114, 1,1-Dichloroethane, 1,1-Dichloroethylene, Freon-113, 1,2-Dibromoethane, 1,2-Dichloroethane, Chloroethane, Tetrachloroethylene, Trichloroethylene, Vinyl chloride, cis-1,2-Dichloroethylene, trans-1,2-Dichloroethylene, trans-1,3-Dichloropropene, Chlorobenzene, o-Dichlorobenzene, m-Dichlorobenzene, Vinyl acetate, Methyl isobutyl ketone
Constraints	Factor 1 (Evaporative emission) Pull Down Maximally (5 % dQ): Benzene, Toluene, Isoprene Factor 3 (Non-vehicular sources) Pull Down Maximally (5 % dQ): n-Butane, i-Butane, n-Pentane, i-Pentane, n-Octane, n-Nonane, n-Decane, n-Undecane, n-Dodecane, Ethylene, Propene, Toluene, Acetylene

162

Table S4. The θ angles (°) among the source profiles at different altitudes in this study.

VOC sources	4750 m	4200 m	3600 m	3400 m	3000 m	2000 m
4750 m	0	19	21	18	49	21
4200 m		0	12	18	41	29
3600 m			0	19	42	31
3400 m				0	40	22
3000 m					0	50
2000 m						0

Table S5. The θ angles (°) among the different source profiles in previous studies.

The θ angles (°)	Gasoline vapors[a]	Gasoline vehicle exhaust[b]	Low altitude tunnel[c]
Gasoline vapors[a]	0	50	41
Gasoline vehicle exhaust[b]		0	18
Low altitude tunnel[c]			0

[a]Average profiles of gasoline vapors derived from SHED tests (Harley et al., 2000; Na et al., 2004; Liu et al., 2008; Zhang et al., 2013; Wu et al., 2015; Man et al., 2020; Sun et al., 2021)

[b]Average profiles of gasoline vehicle exhaust derived from dynamometer tests (Schauer et al., 2002; Na et al., 2004; Guo et al., 2011; Gao et al., 2012; Ou et al., 2014; Li et al., 2019; Wang et al., 2022)

[c]Average profiles of vehicular emissions derived from low-altitude tunnel measurements (Staehelin et al., 1998; Hwa et al., 2002; Zhang et al., 2018b; Chiang et al., 2007; Gentner et al., 2013; Zhang et al., 2018a; Sun et al., 2019; Feng et al., 2021; Song et al., 2020; Jin et al., 2021; Song et al., 2018)

177 **Table S6.** The relative contribution (%) of each species in the PMF source apportionment and NNLS regression results.

Species	PMF Evaporative emissions	PMF Tailpipe exhaust	PMF Non-vehicular sources	NNLS Evaporative emissions	NNLS Tailpipe exhaust	NNLS Non-vehicular sources
Ethane	0	92	7.6	0	95	5.1
Propane	27	31	42	4.4	78	17
n-Butane	88	11	0.8	100	0	0
i-Butane	86	10	4.4	52	48	0
n-Pentane	87	12	1.6	71	29	0
i-Pentane	88	10	1.4	64	36	0
Cyclopentane	81	11	8.3	90	10	0
2,2-Dimethylbutane	72	27	1.2	97	2.7	0
2,3-Dimethylbutane	86	14	0	100	0	0
2-Methylpentane	86	14	0	100	0	0
3-Methylpentane	86	14	0	100	0	0
Cyclohexane	79	18	3.1	35	65	0
Methylcyclopentane	83	16	1.0	100	0	0
n-Hexane	79	14	6.6	45	55	0
2,3-Dimethylpentane	77	22	1.4	83	17	0
2,4-Dimethylpentane	72	22	5.3	35	65	0
2-Methylhexane	78	21	1.1	96	4.5	0
3-Methylhexane	76	22	1.6	77	23	0
Methylcyclohexane	63	31	5.9	100	0	0
n-Heptane	71	27	2.2	62	38	0
2,2,4-Trimethylpentane	75	25	0	100	0	0

2,3,4-Trimethylpentane	54	46	0	99	1.5	0
2-Methylheptane	60	38	2.0	56	44	0
3-Methylheptane	59	39	2.4	59	41	0
n-Octane	56	44	0	100	0	0
n-Nonane	31	69	0	12	88	0
n-Decane	7.5	92	0	2.2	98	0
n-Undecane	4.2	96	0	1.2	99	0
n-Dodecane	5.4	95	0	1.1	99	0
Ethylene	0	100	0	0.0	100	0
Propene	5.3	95	0	0.5	99	0
1,3-Butadiene	74	26	0	50	50	0
1-Butene	86	14	0	55	45	0
cis-2-Butene	89	10	0	100	0	0
trans-2-Butene	89	11	0	77	23	0
1-Pentene	88	12	0	68	32	0
Isoprene	0	64	36	8.9	57	35
cis-2-Pentene	89	11	0	100	0	0
trans-2-Pentene	90	10	0	100	0	0
1-Hexene	84	16	0.6	44	56	0
Acetylene	6.2	94	0	11	89	0
Benzene	6.2	93	1.1	11	88	1.1
Toluene	0	77	23	13	78	8.7
Ethylbenzene	26	56	19	25	48	27
o-Xylene	26	61	13	23	58	19
m/p-Xylene	30	58	12	26	57	17
1,2,3-Trimethylbenzene	14	84	2.4	12	80	8.2

1,2,4-Trimethylbenzene	18	81	1.1	17	76	6.6
1,3,5-Trimethylbenzene	21	77	1.9	21	74	5.4
n-Propylbenzene	27	68	5.5	22	71	7.1
i-Propylbenzene	22	54	24	28	41	32
o-Ethyltoluene	21	75	3.9	19	74	6.9
m-Ethyltoluene	21	79	0	21	76	3.2
p-Ethyltoluene	25	74	0.6	26	71	3.3
Chloroform	27	16	57	5.8	87	7.4
Chloromethane	24	47	29	26	74	0
Dichloromethane	6.6	12	81	2.7	89	8.1
1,1,2-Trichloroethane	46	48	5.4	2.3	98	0
1,2-Dichloropropane	0	35	65	2.5	77	20
p-Dichlorobenzene	7.6	38	54	8.0	50	42
Ethanol	13	14	73	34	44	22
Acetone	16	36	48	8.3	82	10
Acrolein	64	33	3.6	72	22	6.8
2-Butanone	11	24	65	38	56	5.9
Tetrahydrofuran	75	21	4.1	52	41	7.1
Methyl tertiary-butyl ether	89	11	0	100	0	0

178

179 **Table S7.** The contribution proportion (%) of all tunnels and various altitude in the
180 PMF source apportionment results.

Altitude (m)	Evaporative emissions	Tailpipe exhaust	Non-vehicular sources
2000	51	36	13
3000	42	33	25
3400	53	28	19
3600	77	16	8
4200	67	25	8
4750	72	19	9
All tunnels	67	24	9

181

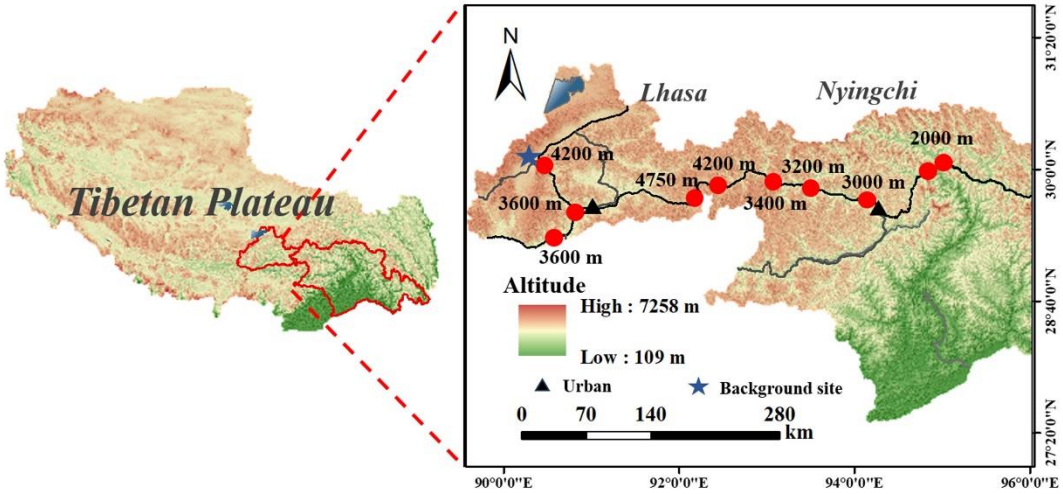

Figure S1. Map distribution of tunnels at different altitudes in this study.

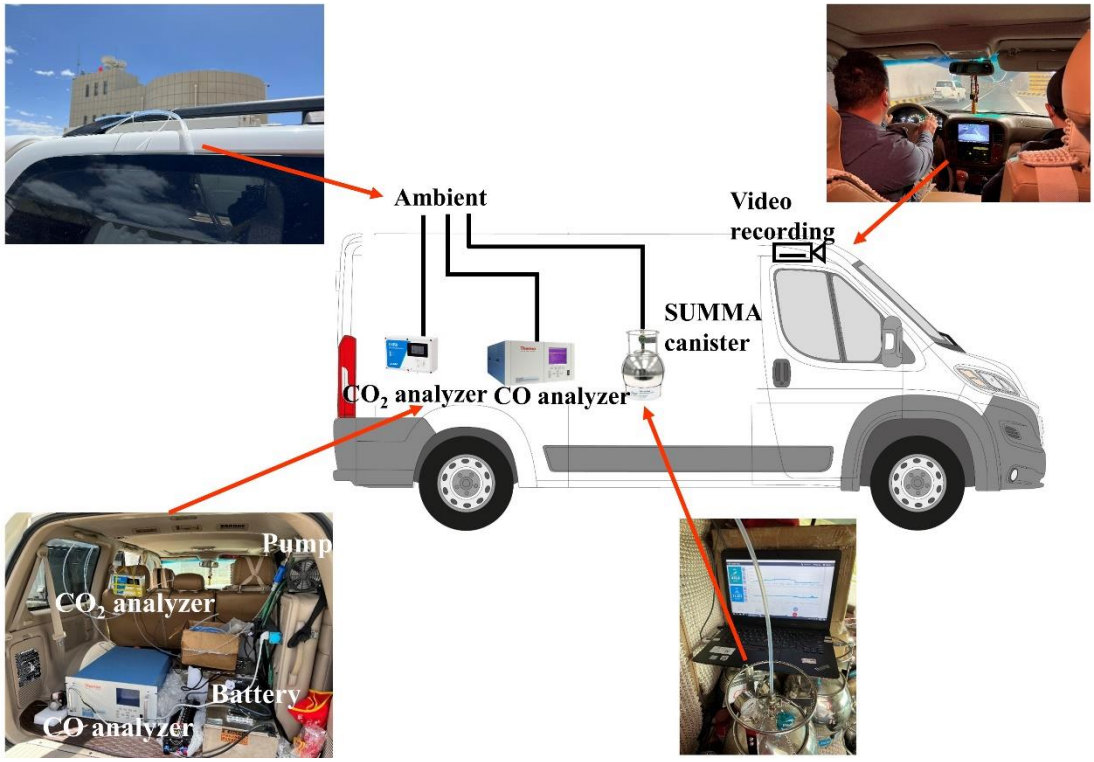

Figure S2. Mobile measurement system design diagram.

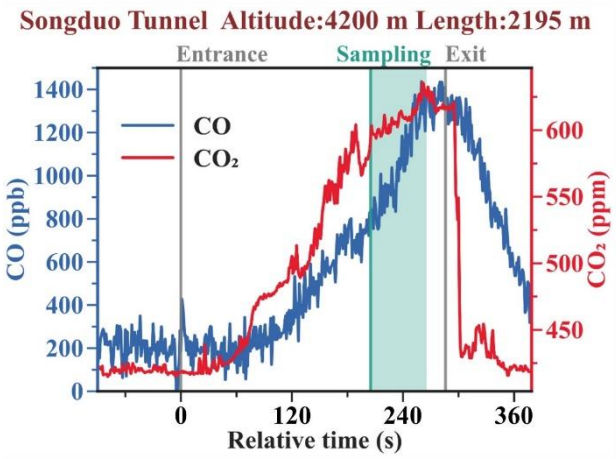

189

190 **Figure S3.** The time series plots of CO and CO_2 concentrations in representative tunnels.
191 The two solid gray lines represent the entrance and exit of the tunnel. The green solid
192 line and shaded area indicate the sampling time when the summa canister was opened.
193 The shaded region represents a 1-min sampling duration of the canister. The time axis
194 has been normalized, with the time of entering the tunnel set as 0 s.

195

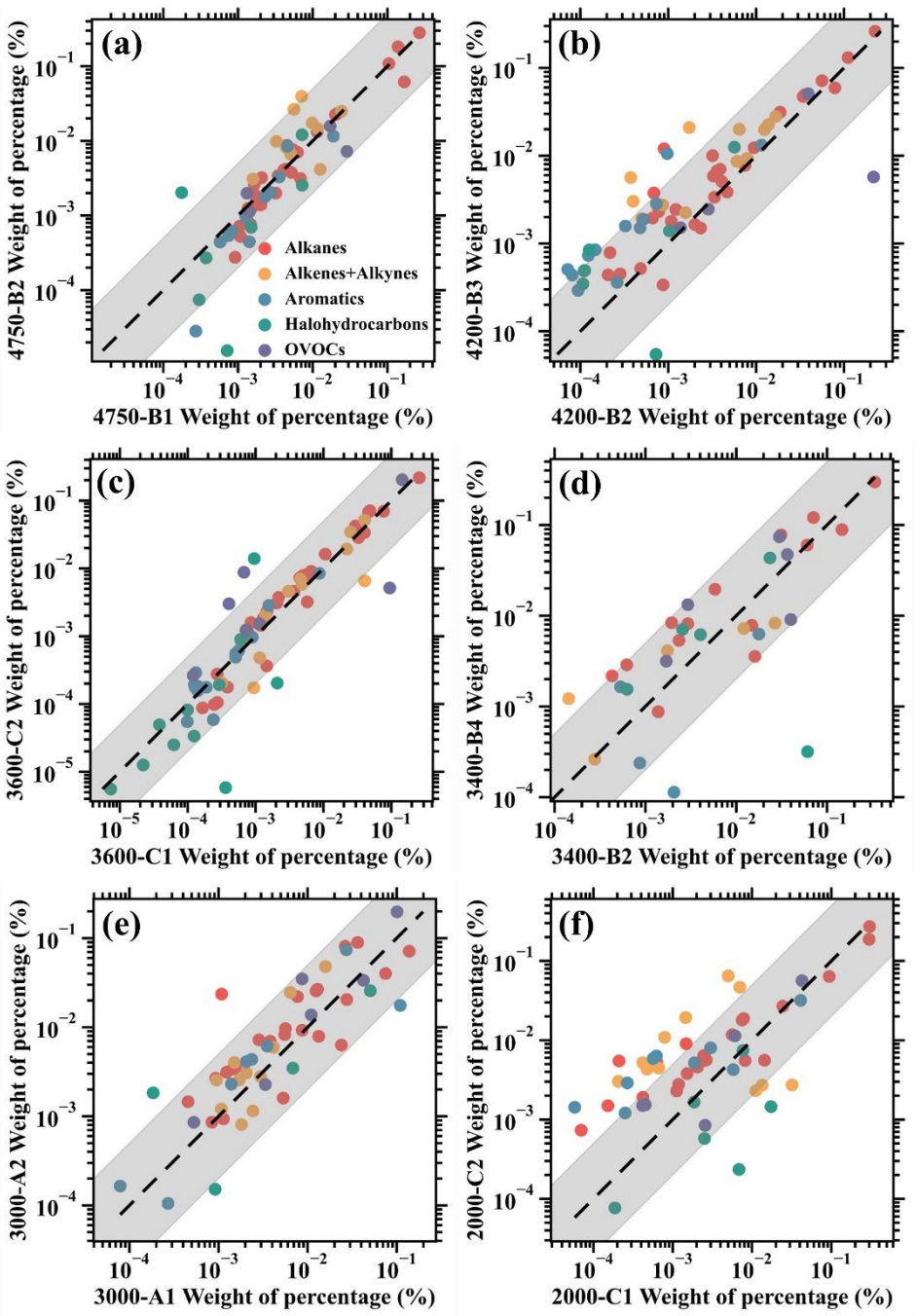

Figure S4. Source profile consistency in the same direction across various altitudes in a tunnel. This figure delineates the source profile fitting results for samples collected in the same direction in a specific tunnel, at different altitudes, (a) through (f) correspond sequentially to the fitted source profiles at each altitude, from 4750 m to 2000 m.

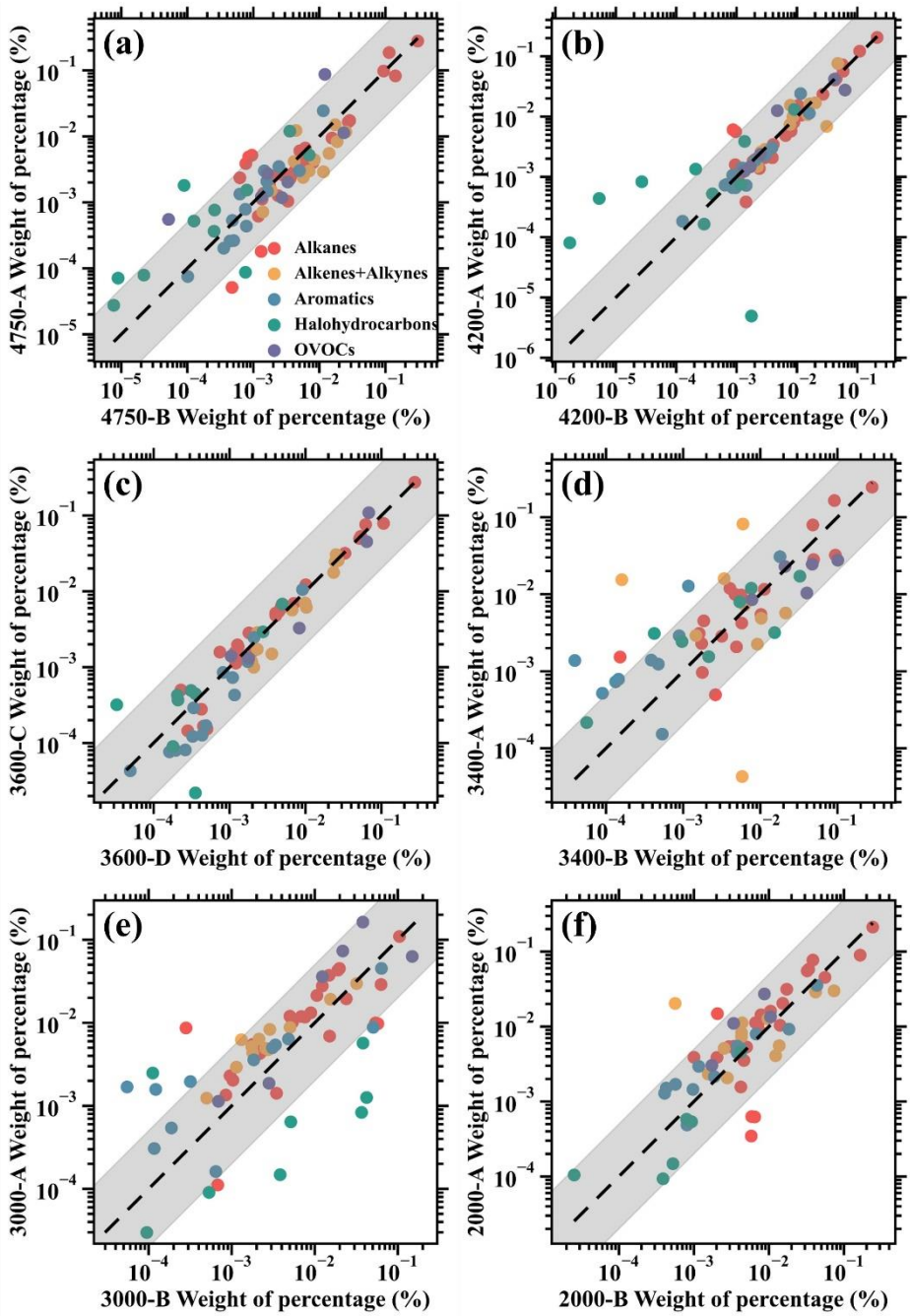

Figure S5. Consistency of source profiles across different directions and altitudes in a tunnel. This figure presents the source profile fitting results for samples collected at various altitudes and in different directions in a specific tunnel, (a) through (f) correspond sequentially to the fitted source profiles at each altitude, from 4750 m to 2000 m.

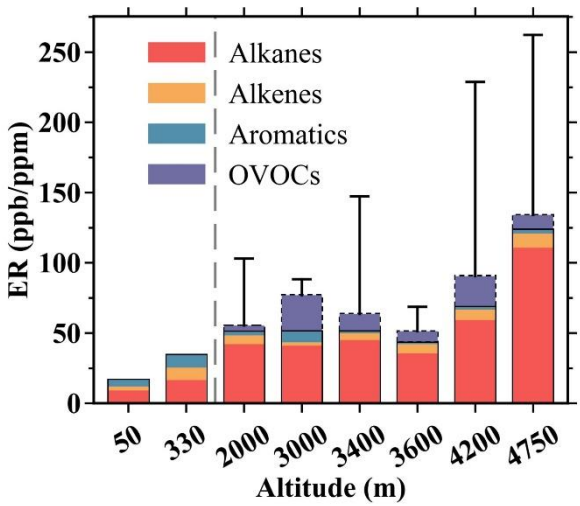

Figure S6. Altitudinal trends in different VOC components, stacked plot illustrating variations in ER with altitude. The gray dashed line on the left side represents results from other studies conducted in low-altitude tunnels. Specifically, data at 330 m are from the Chung-Liao tunnel in Taiwan (Chiang et al., 2007), and at 50 m from the Shing Mum tunnel in Hong Kong (Ho et al., 2009).

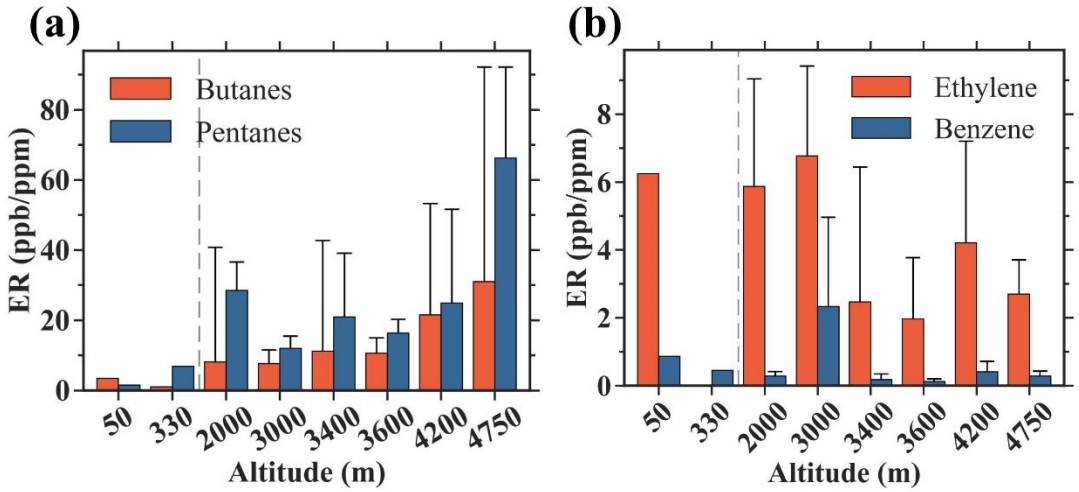

Figure S7. Variation trends of ER for representative species with altitude. (a) The trends in ER for butanes and pentanes. (b) The trends in ER for ethylene and benzene. Data at 330 m are from the Chung-Liao tunnel in Taiwan (Chiang et al., 2007), and at 50 m from the Shing Mum tunnel in Hong Kong (Ho et al., 2009).

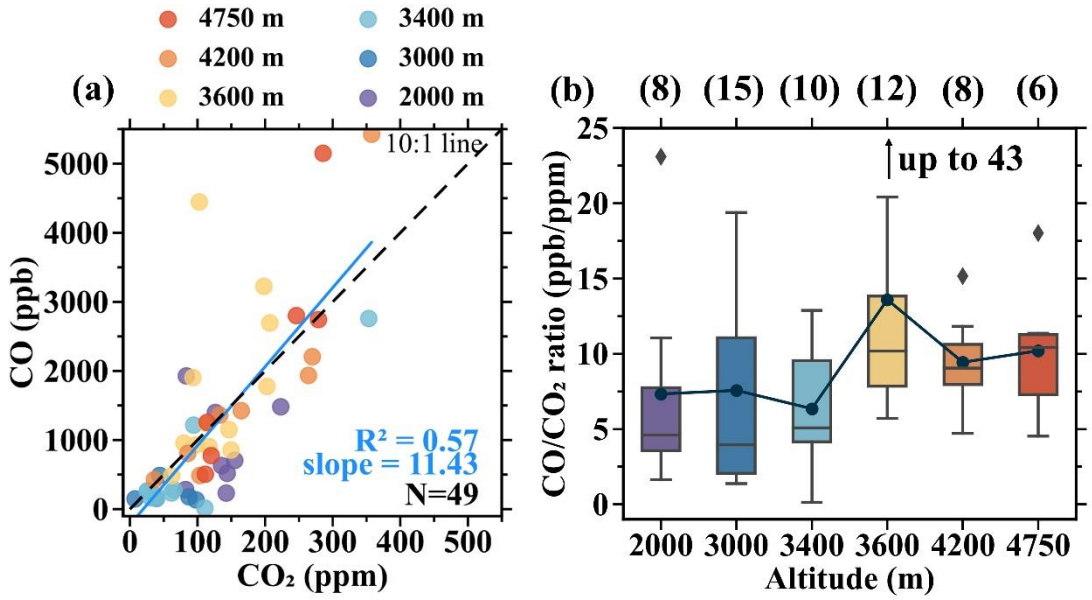

Figure S8. Variations in combustion efficiency (CO/CO_2) from altitudes of 4750 m to 2000 m. (a) The scatter plots depicting the average concentrations of CO versus CO_2 within the tunnel are presented individually. (b) The trend of CO/CO_2 ratios at different altitudes. Different colors denote varying altitudes, with diamond symbols marking outliers beyond 1.5 times the interquartile range and numbers in parentheses representing corresponding sample quantities.

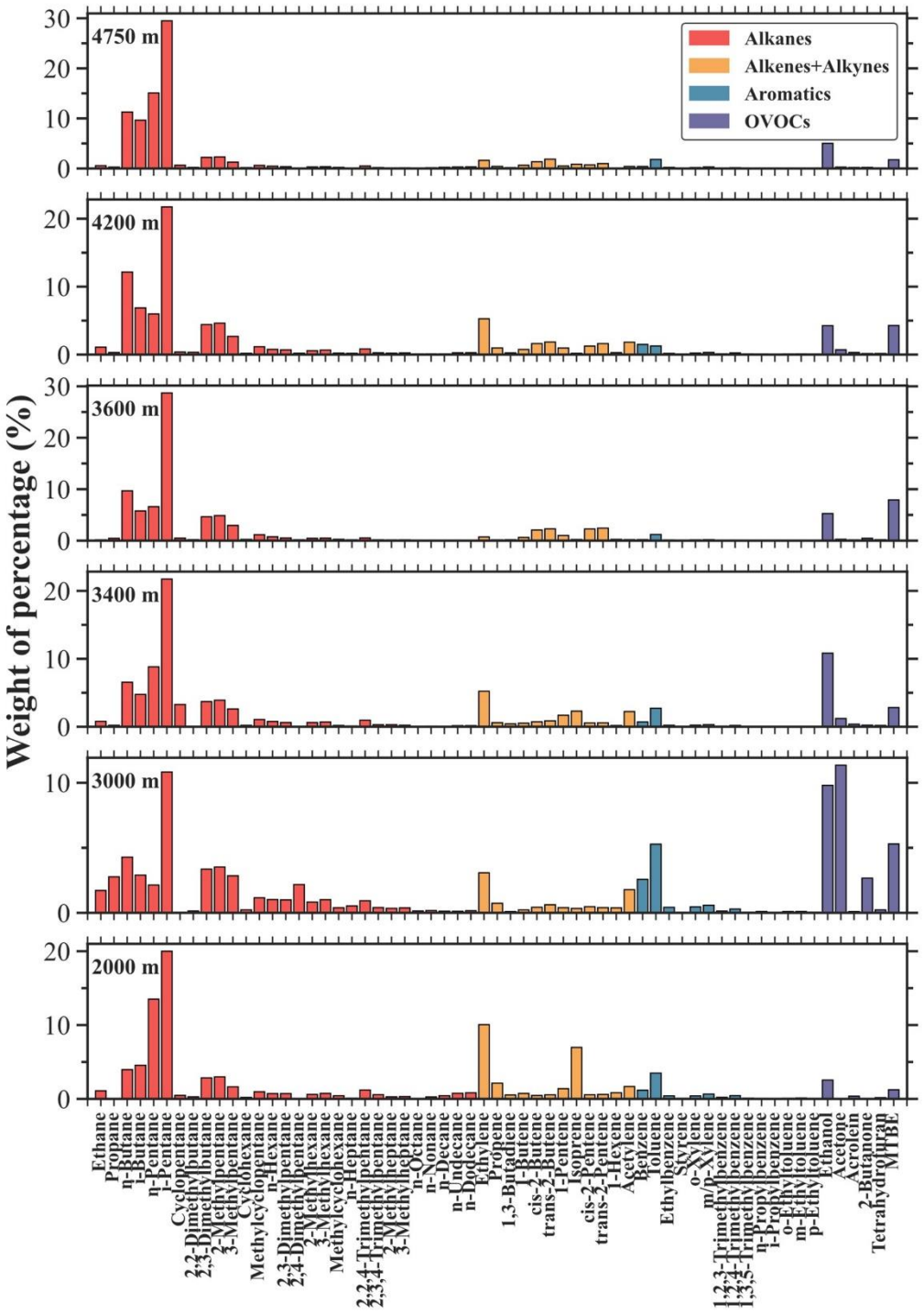

231

232 **Figure S9.** The source profiles of tunnels at different altitudes in this study. These

233 profiles depict the relative contribution percentage by mass of various VOC species in

234 the tunnels.

235

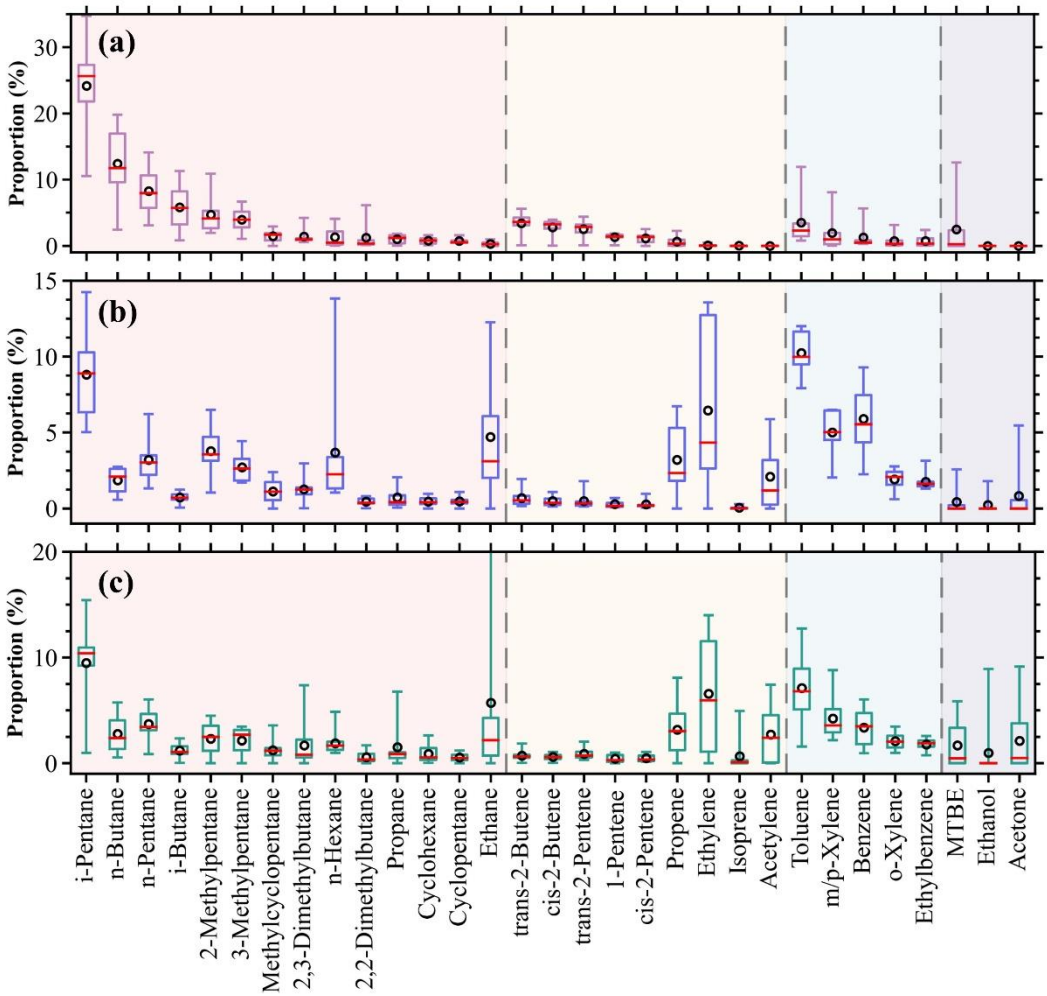

Figure S10. Source profiles from previous studies. (a) Gasoline vapors profiles from the SHED test results (Harley et al., 2000; Na et al., 2004; Liu et al., 2008; Zhang et al., 2013; Wu et al., 2015; Man et al., 2020; Sun et al., 2021). (b) Gasoline vehicle exhaust profiles from chassis dynamometer test results (Schauer et al., 2002; Na et al., 2004; Guo et al., 2011; Gao et al., 2012; Ou et al., 2014; Li et al., 2019; Wang et al., 2022). (e) Tunnel profiles from low-altitude tunnel measurements (Staehelin et al., 1998; Hwa et al., 2002; Zhang et al., 2018b; Chiang et al., 2007; Gentner et al., 2013; Zhang et al., 2018a; Sun et al., 2019; Feng et al., 2021; Song et al., 2020; Jin et al., 2021; Song et al., 2018). The background colors of red, yellow, blue, and purple represent alkanes, alkenes, aromatics, and OVOCs, respectively.

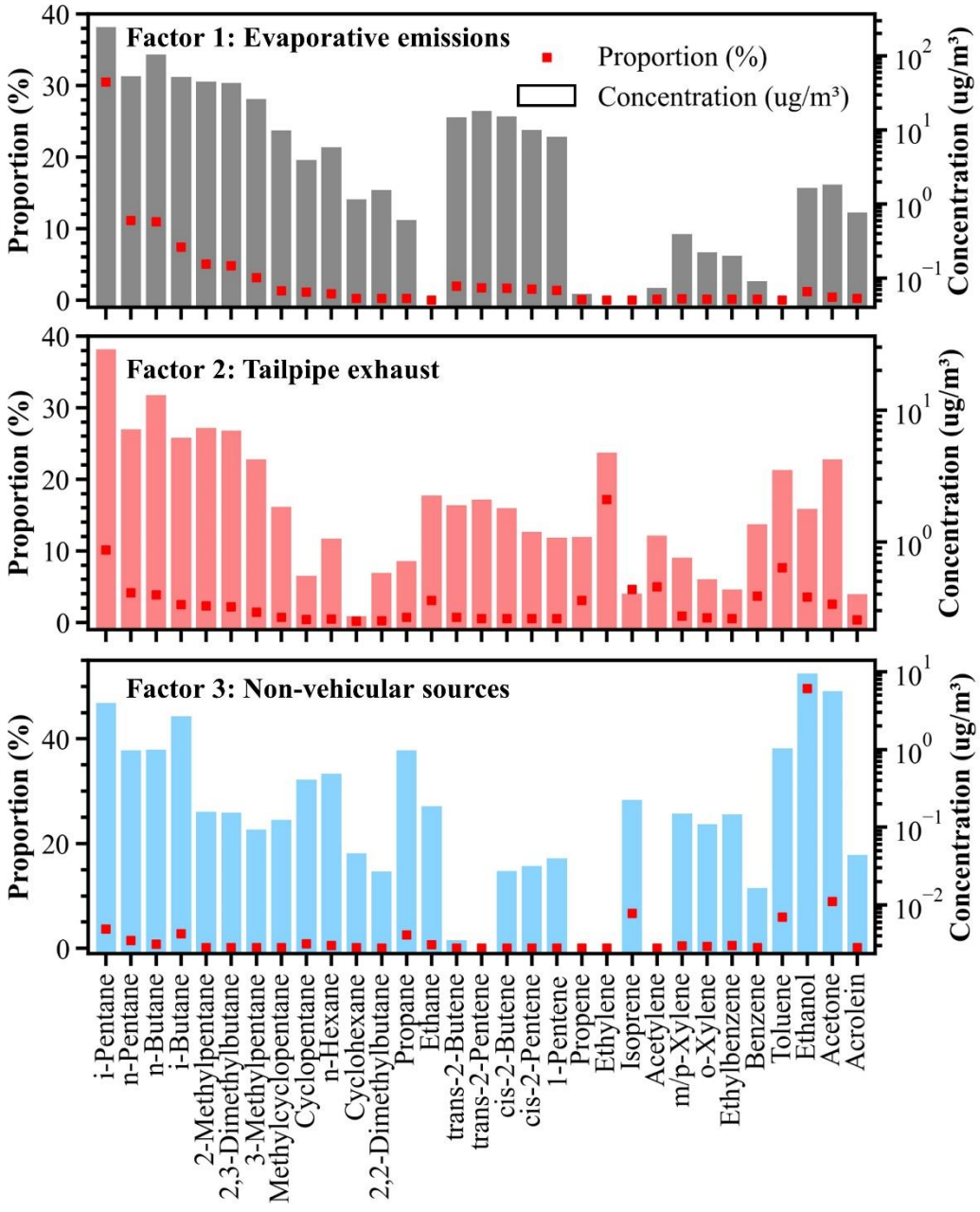

Figure S11. PMF source profiles and concentration. The red square dots represent the VOCs contributions from different sources (%), while the bar chart represents the concentration (ug/m^3).

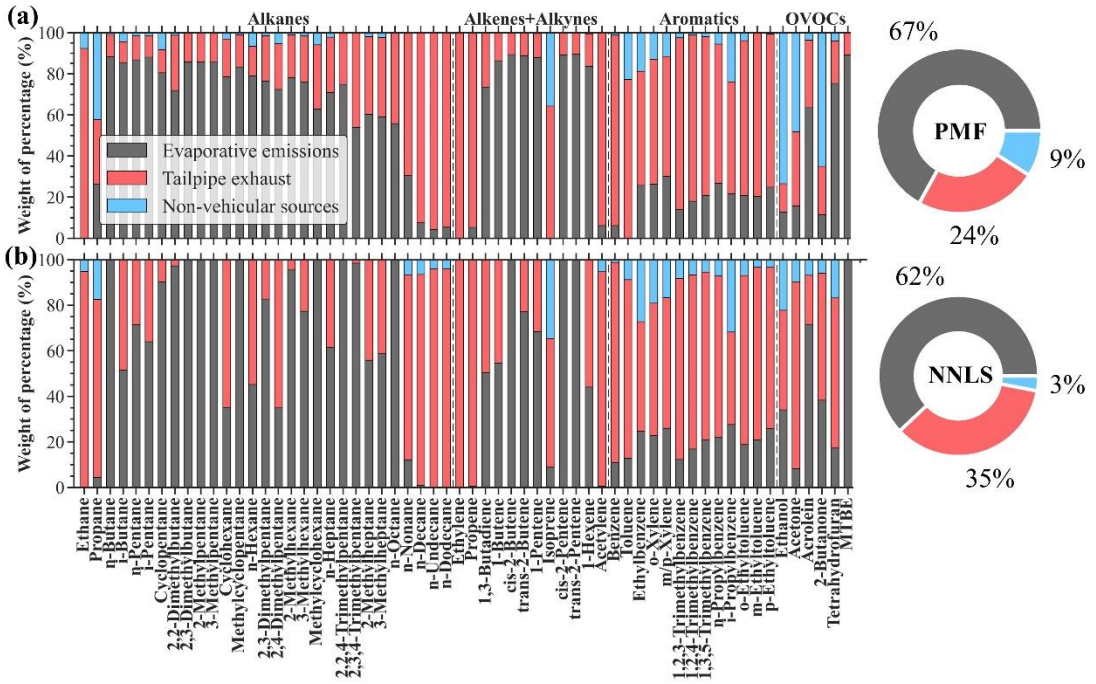

Figure S12. Relative contributions of VOC species sources identified in this study. (a) The results from PMF source apportionment, identifying three primary sources of VOCs with their respective contribution percentages: evaporative emissions (67%), tailpipe exhaust (24%), and non-vehicular sources (9%). (b) The results from NNLS analysis, revealing a different distribution of source contributions: evaporative emissions (62%), tailpipe exhaust (35%), and non-vehicular sources (3%).

Figure S13. Screenshot of the driving recorder at the tunnel. (a) The bangga tunnel at 3600 m was affected by a high-emission event during a canister sampling period due to heavy diesel vehicle traffic, (b) the mila mountain tunnel is located at an altitude of 4750 m, with sparse vegetation near the tunnel entrance, (c) and (d) the parlung No. 1 tunnel is a mountain crossing tunnel surrounded by abundant vegetation, situated at an altitude of 2000 m. Additionally, it operates as a two-way tunnel, allowing traffic to flow in opposite directions.

Reference

Royal Society of Chemistry. ChemSpider | Search and share chemistry: https://www.chemspider.com/, last access: 2025-2-17.

Chiang, H. L., Hwu, C. S., Chen, S. Y., Wu, M. C., Ma, S. Y., and Huang, Y. S.: Emission factors and characteristics of criteria pollutants and volatile organic compounds (VOCs) in a freeway tunnel study, Sci. Total. Environ., 381, 200-211, https://doi.org/10.1016/j.scitotenv.2007.03.039, 2007.

Du, Z. F., Hu, M., Peng, J. F., Zhang, W. B., Zheng, J., Gu, F. T., Qin, Y. H., Yang, Y. D., Li, M. R., Wu, Y. S., Shao, M., and Shuai, S. J.: Comparison of primary aerosol emission and secondary aerosol formation from gasoline direct injection and port fuel injection vehicles, Atmos. Chem. Phys., 18, 9011-9023, https://doi.org/10.5194/acp-18-9011-2018, 2018.

Feng, M., Hu, X., Zhou, L., Zhang, T. Y., Zhang, X., Tan, Q. N., Zhou, Z. H., Deng, Y., Song, D. L., and Huang, C. M.: Real-World Vehicle Volatile Organic Compound Emissions and Their Source Profile in Chengdu Based on a Roadside and Tunnel Study, Atmosphere, 12, 13, https://doi.org/10.3390/atmos12070861, 2021.

Gao, S., Jin, L., Shi, J., Han, B., Wang, X., Peng, Y., Zhao, L., and Bai, Z.: VOCs emission characteristics and emission factors of light-duty gasoline vehicles with bench test (in Chinese), China-Environ. Sci., 32, 397-405, 2012.

Gentner, D. R., Worton, D. R., Isaacman, G., Davis, L. C., Dallmann, T. R., Wood, E. C., Herndon, S. C., Goldstein, A. H., and Harley, R. A.: Chemical Composition of Gas-Phase Organic Carbon Emissions from Motor Vehicles and Implications for Ozone Production, Environ. Sci. Technol., 47, 11837-11848, https://doi.org/10.1021/es401470e, 2013.

Guo, H., Zou, S. C., Tsai, W. Y., Chan, L. Y., and Blake, D. R.: Emission characteristics of nonmethane hydrocarbons from private cars and taxis at different driving speeds in Hong Kong, Atmos. Environ., 45, 2711-2721, https://doi.org/10.1016/j.atmosenv.2011.02.053, 2011.

297 Harley, R. A., Coulter-Burke, S. C., and Yeung, T. S.: Relating liquid fuel and headspace
298 vapor composition for California reformulated gasoline samples containing ethanol,
299 Environ. Sci. Technol., 34, 4088-4094, https://doi.org/10.1021/es0009875, 2000.
300 Ho, K. F., Lee, S. C., Ho, W. K., Blake, D. R., Cheng, Y., Li, Y. S., Ho, S. S. H., Fung,
301 K., Louie, P. K. K., and Park, D.: Vehicular emission of volatile organic compounds
302 (VOCs) from a tunnel study in Hong Kong, Atmos. Chem. Phys., 9, 7491-7504,
303 https://doi.org/10.5194/acp-9-7491-2009, 2009.
304 Hwa, M. Y., Hsieh, C. C., Wu, T. C., and Chang, L. F. W.: Real-world vehicle emissions
305 and VOCs profile in the Taipei tunnel located at Taiwan Taipei area, Atmos. Environ.,
306 36, 1993-2002, https://doi.org/10.1016/s1352-2310(02)00148-6, 2002.
307 Jin, B. Q., Zhu, R. C., Mei, H., Wang, M. L., Zu, L., Yu, S. J., Zhang, R. Q., Li, S. Y.,
308 and Bao, X. F.: Volatile organic compounds from a mixed fleet with numerous E10-
309 fuelled vehicles in a tunnel study in China: Emission characteristics, ozone formation
310 and secondary organic aerosol formation, Environ. Res., 200, 10,
311 https://doi.org/10.1016/j.envres.2021.111463, 2021.
312 Li, W., Sha, Q. e., Yuan, Z., Wang, R., Lin, X., Zheng, J., and Shao, M.: Emission
313 characteristics of VOCs from light-duty gasoline vehicles at constant speed in the Pearl
314 River Delta (in Chinese), Acta. Sci. Circumst., 39, 243-251,
315 https://doi.org/10.13671/j.hjkxxb.2018.0340, 2019.
316 Liu, Y., Shao, M., Fu, L. L., Lu, S. H., Zeng, L. M., and Tang, D. G.: Source profiles of
317 volatile organic compounds (VOCs) measured in China: Part I, Atmos. Environ., 42,
318 6247-6260, https://doi.org/10.1016/j.atmosenv.2008.01.070, 2008.
319 Man, H. Y., Liu, H., Niu, H., Wang, K., Deng, F. Y., Wang, X. T., Xiao, Q., and Hao, J.
320 M.: VOCs evaporative emissions from vehicles in China: Species characteristics of
321 different emission processes, Env. Sci. Ecotechnol., 1, 11,
322 https://doi.org/10.1016/j.ese.2019.100002, 2020.
323 Na, K., Kim, Y. P., Moon, I., and Moon, K. C.: Chemical composition of major VOC
324 emission sources in the Seoul atmosphere, Chemosphere, 55, 585-594,
325 https://doi.org/10.1016/j.chemosphere.2004.01.010, 2004.

Ou, J., Feng, X., Liu, Y., Gao, Z., Yang, Y., Zhang, Z., Wang, X., and Zheng, J.: Source characteristics of VOCs emissions from vehicular exhaust in the Pearl River Delta region (in Chinese), Acta. Sci. Circumst., 34, 826-834, https://doi.org/10.13671/j.hjkxxb.2014.0614, 2014.

Paatero, P. and Tapper, U.: Positive matrix factorization: A non‐negative factor model with optimal utilization of error estimates of data values, Environmetrics, 5, 111-126, https://doi.org/10.1002/env.3170050203, 1994.

Schauer, J. J., Kleeman, M. J., Cass, G. R., and Simoneit, B. R. T.: Measurement of emissions from air pollution sources. 5. C_1-C_{32} organic compounds from gasoline-powered motor vehicles, Environ. Sci. Technol., 36, 1169-1180, https://doi.org/10.1021/es0108077, 2002.

Song, C., Ma, C., Zhang, Y., Wang, T., Wu, L., Wang, P., Liu, Y., Li, Q., Zhang, J., and Dai, Q.: Heavy-duty diesel vehicles dominate vehicle emissions in a tunnel study in northern China, Sci. Total. Environ., 637, 431-442, https://doi.org/10.1016/j.scitotenv.2018.04.387, 2018.

Song, C. B., Liu, Y., Sun, L. N., Zhang, Q. J., and Mao, H. J.: Emissions of volatile organic compounds (VOCs) from gasoline- and liquified natural gas (LNG)-fueled vehicles in tunnel studies, Atmos. Environ., 234, 13, https://doi.org/10.1016/j.atmosenv.2020.117626, 2020.

Staehelin, J., Keller, C., Stahel, W., Schläpfer, K., and Wunderli, S.: Emission factors from road traffic from a tunnel study (Gubrist tunnel, Switzerland). Part III: Results of organic compounds, SO_2 and speciation of organic exhaust emission, Atmos. Environ., 32, 999-1009, https://doi.org/10.1016/S1352-2310(97)00339-7, 1998.

Sun, L., Liu, Y., Zhao, J., Sun, S., Song, C., Zhang, J., Li, Y., Lin, Y., Wang, T., and Mao, H.: Pollution Characteristics and Emission Factors of VOCs from Vehicle Emissions in the Tianjin Tunnel (in Chinese), Environ. Sci-China, 40, 104-113, https://doi.org/10.13227/j.hjkx.201804187, 2019.

Sun, L. N., Zhong, C. Z., Peng, J. F., Wang, T., Wu, L., Liu, Y., Sun, S. D., Li, Y. N., Chen, Q., Song, P. F., and Mao, H. J.: Refueling emission of volatile organic compounds

from China 6 gasoline vehicles, Sci. Total. Environ., 789, 10, https://doi.org/10.1016/j.scitotenv.2021.147883, 2021.

Wang, S., Yuan, B., Wu, C., Wang, C., Li, T., He, X., Huangfu, Y., Qi, J., Li, X.-B., and Sha, Q. e.: Oxygenated volatile organic compounds (VOCs) as significant but varied contributors to VOC emissions from vehicles, Atmos. Chem. Phys., 22, 9703-9720, https://doi.org/10.5194/acp-22-9703-2022, 2022.

Wu, Y., Yang, Y. D., Shao, M., and Lu, S. H.: Missing in total OH reactivity of VOCs from gasoline evaporation, Chin. Chem. Lett., 26, 1246-1248, https://doi.org/10.1016/j.cclet.2015.05.047, 2015.

Zhang, Q. J., Wu, L., Fang, X. Z., Liu, M. Y., Zhang, J., Shao, M., Lu, S. H., and Mao, H. J.: Emission factors of volatile organic compounds (VOCs) based on the detailed vehicle classification in a tunnel study, Sci. Total. Environ., 624, 878-886, https://doi.org/10.1016/j.scitotenv.2017.12.171, 2018a.

Zhang, Y. L., Wang, X. M., Zhang, Z., Lü, S. J., Shao, M., Lee, F. S. C., and Yu, J. Z.: Species profiles and normalized reactivity of volatile organic compounds from gasoline evaporation in China, Atmos. Environ., 79, 110-118, https://doi.org/10.1016/j.atmosenv.2013.06.029, 2013.

Zhang, Y. L., Yang, W. Q., Simpson, I., Huang, X. Y., Yu, J. Z., Huang, Z. H., Wang, Z. Y., Zhang, Z., Liu, D., Huang, Z. Z., Wang, Y. J., Pei, C. L., Shao, M., Blake, D. R., Zheng, J. Y., Huang, Z. J., and Wang, X. M.: Decadal changes in emissions of volatile organic compounds (VOCs) from on-road vehicles with intensified automobile pollution control: Case study in a busy urban tunnel in south China, Environ. Pollut., 233, 806-819, https://doi.org/10.1016/j.envpol.2017.10.133, 2018b.